Heide Ibrahim (Autor)

Tracking coherences in a dissipative ocean:
Analysing and controlling Br2/Ar matrix

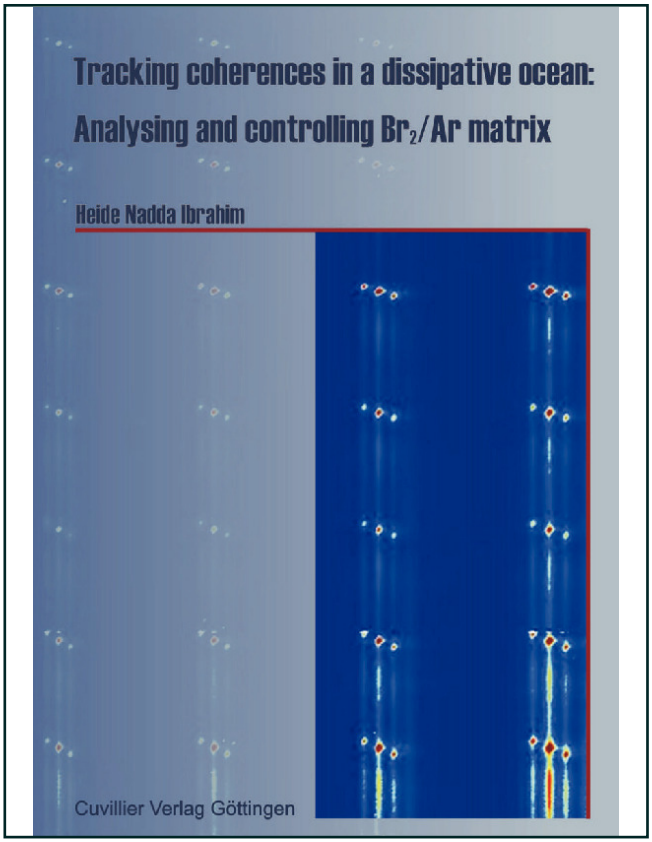

https://cuvillier.de/de/shop/publications/1409

Introduction

"That's funny," said Pooh, throwing sticks into a creek.
"I dropped it on the other side," said Pooh,
"and it came out on this side!
I wonder if it would do it again?"
It did [...]
Then he dropped two in at once,
but as they were both the same size,
he didn't know if it was the one
which he wanted to win,
or the other one.
So the next time he dropped one big one
and one little one.
A. A. Milne
Winnie - the - Pooh

From the very beginning, human beings tend to control their environment - sometimes with, sometimes without analysing the conditions on site, in advance. Environment can mean other creatures, it can be nature in general or - after several thousand years of development - a chemical reaction controlled by light, like in this work. The concept of control is not restricted to the traditional light – matter interaction by varying energy or power of light to yield for example photo-ionisation of molecules. In the past 15 years experiments have advanced to scales, where the quantum nature of systems become more and more apparent [1–4]. This requires sophisticated tools and they are found in femto second (fs, 10^{-15}s) lasers and pulse shapers. These pulses permit one to sample the movements of atoms on fs timescales [5], even combined with atomic spatial resolution [6] in X – ray diffraction. Pulse shapers allow for a computer controlled manipulation of the broad spectral distribution which is incorporated with ultrashort time events. By means of optical Fourier transformation, separated frequencies can be addressed in the Fourier plane. Herewith, nearly arbitrary temporal waveforms can be generated with respect to amplitude, phase and polarisation. Such a toolbox provides the capability to intervene in molecular dynamics and simplify the transient response of a system by enhancing one mode with respect to others due to wave packet interferences [7–13]. This selection is obtained by generating pulse trains which preferentially couple to one mode and this mode can be more and more amplified [14, 15], like in the picture of a child on a swing which is pushed with a period matching to the recurrence time.

A further development is the steering of chemical reactions due to varied compositions of molecular wave packets [16–18]. In the framework of this thesis, predissociation of a diatomic molecule embedded in a rare gas crystal is controlled.

How to find out which waveform is required to accomplish a distinct task? A common technique is the appliance of evolutionary algorithms in experiment [19] or on the theoretical side, optimal control theory (OCT). Both strategies record an observable and try to maximise its value by changing the field parameters, $i.e.$, in experiment a closed loop between computer, shaper and detector. Amazing results are obtained and recently reviewed in [20], however, two difficulties

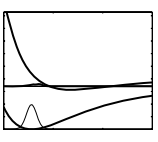

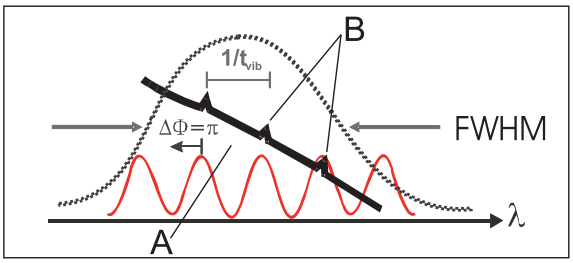

Figure 1: Spectral representation of the light absorption of a molecule when two pulses with a time separation of T_{vib} interfere. The first pulse excites a broad distribution indicated with the dashed envelope. Two pulses lead to a sinusoidal interference pattern (thin solid line). If their relative phase $\Delta\Phi = 0$, the spectral maxima match the vibrational progression on the absorption spectrum (thick solid line). For $\Delta\Phi = \pi$ it is shifted to the minima.

remain: First, one has to prevent the algorithm from getting trapped in a local extremum. And second, it is rather challenging to interpret the composition of the optimised waveform. In contrast, a straightforward strategy was chosen in this work: In tutorial experiments with a Michelson interferometer, time delay and relative phase between the two pulses were scanned and the molecular response due to the changing composition of wave packets was analysed [21]. To gain enhanced selectivity, sequences of several pulses are required, which can include spectral characteristics like the molecular anharmonicity and even shiftings of vibrational levels due to couplings with other electronic states. Access to their generation lies in the frequency domain. There, the vibrational progression which should be enhanced was directly written on the pulse shaper - pixel by pixel, based on a deep spectroscopic analysis [22]. This refrains from a description of complex analytic functions and works successfully, since the right timing and relative phases of the pulse sequence are adapted inevitably.

The halogen bromine, embedded in an argon crystal turned out to be an ideal model system for coherent control experiments. Absorption spectra are dominated by a structureless background labeled A - the dissipative ocean which is indicated in Fig. 1 as thick solid line. Latent coherent signatures marked as B, shown as small peaks on the background, were found in it. The spacing of B is inversely proportional to the vibrational roundtrip time T_{vib}. The aim is to amplify these peaks with pulse sequences designed in phase ($\Delta\Phi$) and amplitude. Each pulse individually excites non - selectively a broad envelope (dashed line). Sharp spectral features are the result of interference effects of several pulses which is indicated with the sinusoidal distribution (thin solid line). Playing with $\Delta\Phi$ allows for a shifting of selected frequencies with respect to the envelope and thus enhancing or attenuating the excitation of the faint coherent features.

The concept of wave packet interference and the required coherences are introduced in Ch. 1. Various knowledge on Br_2/Ar exists on a very high level and is collected in Ch. 2. However, the elaborate control experiments of this work which are introduced in Ch. 3, require even more detailed spectroscopic information concerning intensities, energetic positions or frequency resolution and the literature is contradictory. Thus, detailed frequency resolved experiments in Ch. 4 solving the inconsistencies, and a time resolved analysis in Ch. 5 were prefixed to the final control experiments in Ch. 6.

Two positions of curve crossings of repulsive states with the covalent state B were determined from a two dimensional spectrum of emission $vs.$ excitation wavelength, which covers nearly the whole bound area of the B-state. Sharp zero phonon lines (ZPL), representing the molecular vibrations, and broad phonon side bands (PSB) which were assigned to the crystal's phonon density of states are clearly pronounced. The side bands increase at higher matrix contributions and merge to a continuum. These signatures reveal information on matrix induced predissociation. This knowledge was applied in the control experiments to manipulate the efficiency of population transfer from the B-state to other electronic states. Investigating the bound part of the B potential is com-

plicated due to larger absorption probabilities of the A-state which is matrix bound in this energy region. The A-state interaction with the matrix causes the dominant unmodulated background in Fig. 1. This work succeeded in picking out the faint coherent signatures from the overwhelming background and in controlling matrix induced predissociation. It gives a deep insight into the complex interaction of guest and host and a straightforward method to track weak coherent dynamics in a dissipative ocean.

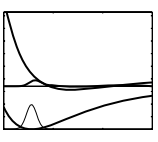

Chapter 1

Coherence and wave packet interferometry

Throughout this whole thesis the idea of Heisenberg's uncertainty principle restrictions will be present. It connects the resolution limits of time and frequency resolved spectroscopy. In the case of time resolved spectroscopy we deal with ultrashort laser pulses on the order of femto seconds (fs, $10^{-15}s$), which necessarily have an energetic width of several hundreds of wave numbers for visible light. Or to speak in molecular language, several vibronic eigenstates are covered by the pulse width. Applying the techniques of frequency resolved spectroscopy leads to the other extreme. The wavelength resolution is strongly enhanced, however, the pulses become long and time resolved information about molecular dynamics is lost.

We are well aware of these phenomena in the limiting cases of long and short pulse durations. In this work it will be tried to combine dynamical measurements with spectrally selected molecular excitation. Coherent control schemes will be applied, which rely on the flexible generation of sharp spectral features, $e.g.$, like a frequency comb whose wavelength and spacing can be adjusted. Therefore, it is of interest in which way the molecular system takes up the information of pulse durations. In Sec. 1.2 it is shown that the molecule does not "know" in the beginning of the control pulse how the electric field of the exciting light will evolve with time and whether it belongs to an ultrashort laser pulse or to a CW source [23, 24]. It does not even "know", whether it is excited in a bound or a repulsive potential. All this information has to develop in time due to interferences of the newly excited wave packet with the already propagating one. In the first moment of excitation the spectrum is comparable to a whitelight continuum.
Sharp spectral features are the result of constructive interferences at spectral maxima and destructive interferences at the minima. They can only be pronounced when the early part of the absorbed light and the late one act on the same conditions, $i.e.$, all coherences are preserved. But these coherences in a molecule will be affected by the presence of an environment. For molecules isolated in a rare gas crystal an electronic and vibrational transition will also lead to an electronic and vibrational coupling of the chromophore with the matrix, since molecule and cage atoms are close together, even in the equilibrium configuration of the ground state.

This chapter is arranged as follows: First, the concept of a wave packet, describing the motions of a molecule in a quantum mechanical way is introduced. Second, the term coherence is described classically and quantum mechanically being the basic requirement for the observation of sharp spectroscopic signatures. Then, the process of light absorption will be discussed in terms of wave packet interferometry. Electronic and vibrational coherences are essential for applying a coherent control of chemical reactions with light. In our case, this control acts on the coupling between the chromophore and the surrounding matrix, treated finally.

1.1 Wave packets

A short laser pulse exciting a molecule coherently couples several energy eigenstates $|\phi_n\rangle$ having their eigenvalues E_n [25, 26], due to its large spectral width. This superposition of eigenstates

leads to a wave packet $|\Psi(t)\rangle$:

$$|\Psi(t)\rangle = \sum_n c_n e^{-i\frac{E_n}{\hbar}t}|\phi_n\rangle, \tag{1.1}$$

with c_n being the excitation coefficients. In general, $|\phi_n\rangle$ can be electronic, vibrational or rotational eigenstates of the molecule, here only the vibrational ones will be treated. The absolute square of a such a vibrational wave packet is called the population of an electronic potential energy surface. A wave packet with the superposition of eigenstates always obeys Heisenberg's uncertainty principle restriction, which is in the time - energy representation:

$$\Delta E\, \Delta t \;\geq\; \hbar/2. \tag{1.2}$$

This requires for an ultrashort event a wide-stretched contribution of eigenstates. In the other extreme, with a long pulse duration it is possible to reduce the energetic width to a single eigenstate. In Sec. 1.2 these ideas will be taken up again.

1.1.1 Franck - Condon principle

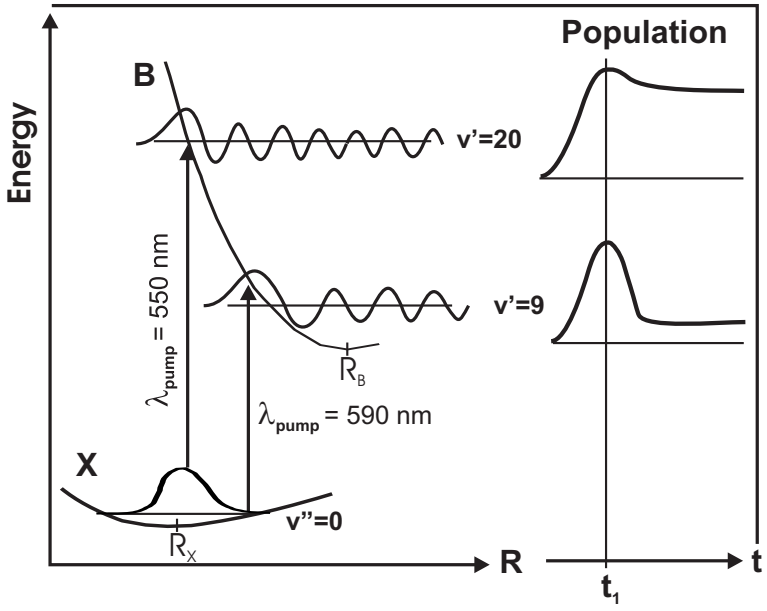

Figure 1.1: Franck - Condon principle with potential parameters of the Br_2 molecule. On the left hand side schematically the excitation of two different transitions X($v''=0$)→B($v'=9$) and X($v''=0$)→B($v'=20$) is displayed. R_X and R_B are the equilibrium internuclear distances. On the right hand side a plot of created population of the B-state $vs.$ time is given, where t_1 is the centre of excitation pulse.

The probability for transitions from a vibrational level v'' of the electronic ground state X to vibrational levels v' of an electronically excited state B depends on the overlap of wave functions of both states.

Figure 1.1 demonstrates the Franck - Condon (FC) principle with two different excitation energies shown on the left hand side. The specific numbers for wavelength and vibrational levels are chosen for the Br_2/Ar potentials. However, at this point they are not of major importance. In the case of bromine, the potential minima for ground and excited state are not at the same position and the equilibrium internuclear distance changes during the electronic excitation from R_X to R_B. On the ground state X the quantum mechanical wave function for $v''=0$ is plotted, the only occupied level in our case, having its maximum in the centre, at R_X, where the classical kinetic energy E_{kin}

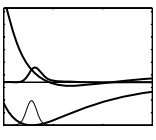

of the atoms is maximal. This is in contrast with the classical picture, where the largest probability of residence is expected to be at the turning points. For higher vibrational levels sketched on the electronically excited potential B, the expectation values better approximate this classical picture. The probability $P(\chi_{v''}, \chi_{v'})$ of a vibronic transition X($v'' = 0$)→B(v') is calculated in the Condon approximation with constant electronic transition moment by the FC overlap integral [27] with the nuclear vibrational functions of ground state X $\chi_{v''}(R)$ and excited electronic state B $\chi_{v'}(R)$:

$$P(\chi_{v''}, \chi_{v'}) \; = \; \int \chi_{v''}(R)\, \chi_{v'}(R)\, dR, \tag{1.3}$$

and integrating over the complete internuclear distance R. In the case of bromine, the transition to $v' = 20$ with $\lambda_{pump} = 550$ nm is close to the FC maximum. This can be immediately seen since the maxima of both wave functions are centred on top of each other. For the excitation at lower energy $\lambda_{pump} = 590$ nm, again the maximum in the $v' = 9$ wave function is met, however only in the far wing of the Gaussian wave function of the ground state and thus the value of the FC integral, called the FC factor, decreases dramatically. This effect will be part of the discussions in the experimental chapters, since the experiments utilize this energetic region. The gas phase FC factors of bromine are given in Fig. 4.20. The way in which the probability factors effect the population of an excited state versus time is demonstrated at the right hand side in Fig. 1.1 for a pulse that is short compared to the vibrational roundtrip time. Population is increasing as long as the intensity of the excitation pulse is increasing (until the envelope reaches a maximum) and this time is marked with t_1. For the transition close to the FC maximum $\lambda_{pump} = 550$ nm the excitation is called $resonant$ and nearly all population pumped into the B-state remains there when the pulse amplitude is decreasing. The more an excitation energy deviates from the resonant transition energy, the less population can stay in the excited state due to destructive interference effects at longer times. Instead of a further increase, population is dumped back to the ground state while the pulse is fading. For a $non-resonant$ transition like in the $\lambda_{pump} = 590$ nm case, only a small amount compared to the population reached for the pulse intensity maximum remains. Once the pulse is terminated, the amount of population is fixed. This effect shows up in the wave packet simulations of Sec. 6.3.3.

One idea to increase the population of the excited state accessed by the non – resonant transition would be to burn a hole in the ground state with a first pulse, in order to obtain a propagating wave packet which covers several $v'' > 0$. When the ground state wave packet reaches the outer turning point its expectation value there is raised and a second pulse coming at the right time would benefit from the increased FC factors for this transition [28]. However, an amount of 10-20% of the ground state population would have to be pumped to an upper state until this effect would be significant.

In the simulations discussed in Sec. 5.2.1, the overlap integral is inherently involved and FC factors can be derived.

The discussed control schemes require $coherence$, and this term will be introduced in the next section.

1.2 Coherence

The terminology of coherence, necessary for an understanding of the time resolved control experiments, but also of the frequency resolved spectra, is introduced from the classical point of view. The question to be addressed, is a loss of phase relations in between an ensemble of oscillators [29, 30], representing, $e.g.$, the vibrations of a number of molecules. For simplification the oscillators are treated as harmonic ones, in the beginning.

It is useful to represent this problem in classical phase space where the oscillations can be treated in momentum p $vs.$ space coordinate q in appropriate units. The oscillations follow iso-

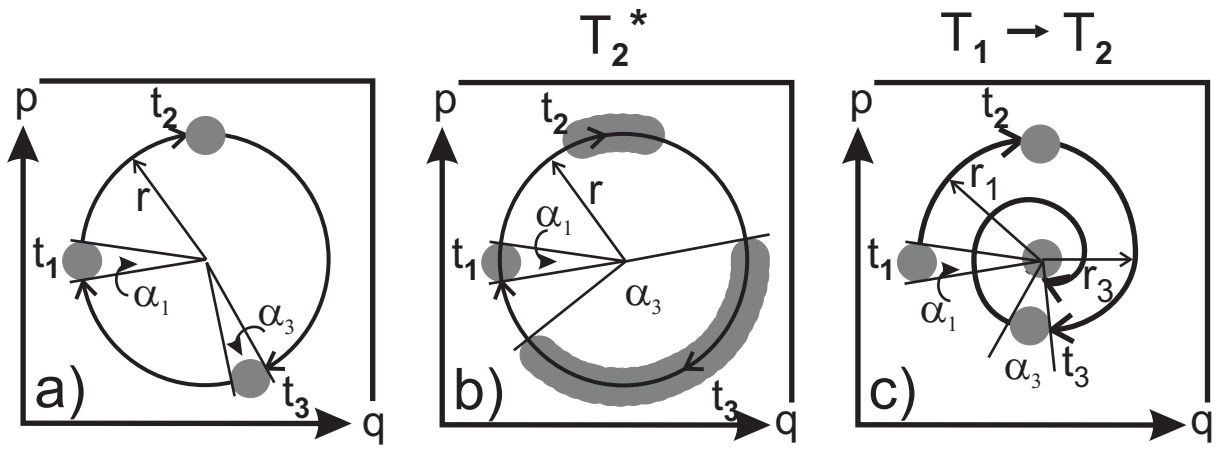

Figure 1.2: A sketch for dephasing is shown with the distribution of an ensemble of free harmonic oscillators at three different times $t_1 < t_2 < t_3$ in phase space with q (position) $vs.$ p (momentum). In the case of $full\ coherence$, $i.e.$, no dissipation or dephasing in a) the shape does not change, the constant energy shell is not left (r = const) and therefore the angle α related to the extension in classical phase space is constant in time. In b) $pure\ dephasing$ is depicted, with a distribution spreading over the course with time and inducing an increase in the angle thus $\alpha_1 < \alpha_3$. $Dissipation$ in c) leads also to an increase in α for the same extension in phase space due to a loss in energy. It spirals down to equilibrium energy in the minimum (r_1<r_3). This figure is adapted from Ref. [26]

energetic circles in these coordinates as long as no energy is lost. Those circles can be described with their radius r, where $r^2 = p^2 + q^2$ starting from the origin of phase space as can be seen in Fig. 1.2. Looking from this centre towards the phase - momentum distribution defines the angle α. Panel a) shows the situation of complete coherence, where no dephasing processes occur. As grey disks the momentum - space distribution of the ensemble of free harmonic oscillators at three different times ($t_1 < t_2 < t_3$) is shown. The ensemble propagates on the iso-energetic circle without changing its shape and thus the reference angle α is constant for all times. In plot b) $pure\ dephasing$, $e.g.$, due to elastic scattering of the molecules is depicted, the dephasing time T_2^* will be introduced soon. The overall energy of the ensemble of oscillators is conserved, therefore it still propagates on the same circle with time. However, different oscillators experience a slight change in phase and the disk of the whole ensemble smears out. For a large time (not shown), the ensemble would completely fill out the circle and $\alpha = 2\pi$; then it is called $fully\ incoherent$. In c) $dissipation$ due to inelastic scattering (concerning this thesis: vibrational energy relaxation) is illustrated where the shape of the distribution disk does not change since no pure dephasing occurs. Whereas, the whole ensemble looses energy and follows a spiral trace down to the centre of phase space. Measuring the angle from the centre, again, α is increasing until it reaches 2π at the end of the spiral, illustrating that dissipation (T_1) leads to dephasing (T_2) as well.

In a real molecular system embedded in a matrix cage one has to deal with different types of coherences and two shall be discussed, exemplified in Fig. 1.3. In a) the loss of electronic coherence is addressed. The cage can act as a static inhomogeneous or moving solvent and cause a relative shift of effective potentials B in energy ΔE and/or internuclear distance ΔR (solid and dotted lines), compared to the ground state X for individual molecules. This leads to electronic dephasing, since the phase will vary in individual transitions to B. The terms $dephasing$ and $decoherence$ are synonymously used and specified in the following.

For the experiments treated here, electronic and vibrational coherence will be necessary as long as the light pulse or pulse train acts on the molecule in order to couple the contributing electronic

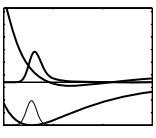

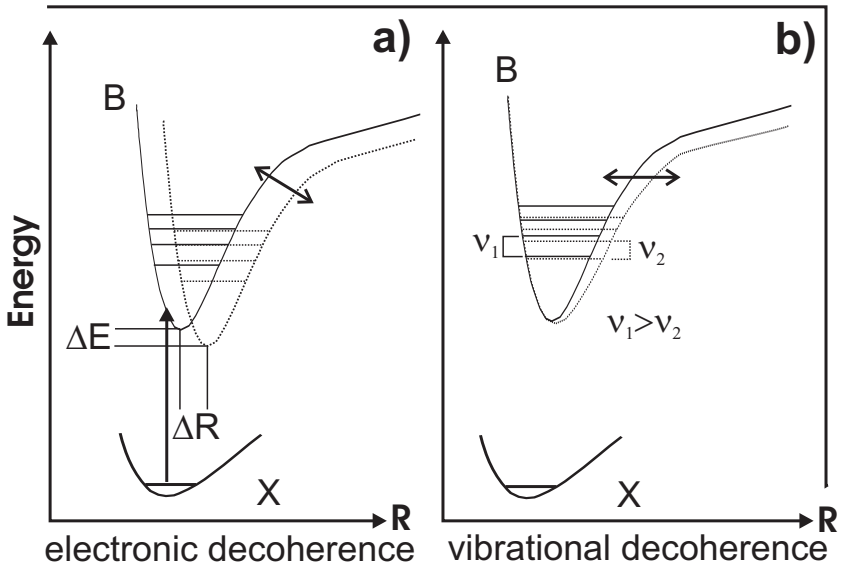

Figure 1.3: Model for electronic and vibrational decoherence. a) electronic coherence strongly depends on a fixed relation between ground state X and excited state B. Cage influence might lead to a shift of the upper potential and thereby the transition energy shifts by ΔE and leads to electronic dephasing. b) vibrational coherence is decoupled from electronic transitions but relies on the vibrational spacing ν. If the cage changes, $e.g.$, the outer wing of the higher lying potential of an ensemble, ν is affected and vibrational dephasing occurs.

states coherently. Only under this condition complete coherent control can be maintained. Depending on the density and symmetry of the environment, the electronic coherence is typically on the order of femto - to picoseconds for condensed systems [17, 21] and thus orders of magnitude shorter than for gas phase systems, as will be discussed in Sec. 2.2.7. In the scheme for electronic decoherence in Fig. 1.3a, the vibrational spacing of the oscillators is not affected, since the potential energy surface is not deformed. Therefore, vibrational coherence is preserved. Figure 1.3b shows a possible scenario for vibrational decoherence. Now, due to a change in the surrounding cage, the outer wing of the effective potential B (solid line) with vibrational spacing ν_1 may be flattened (dotted line) into another oscillator with smaller vibrational spacing ν_2. In that case, the ensemble of oscillators will no longer vibrate with one and the same period and this will cause decoherence and a line broadening of the spectroscopic signature corresponding to this vibration. Two kinds of line broadening have to be explained: Homogeneous broadening occurs for all members of an ensemble in the same way, in our case, due to a similar cage influence. Another effect is inhomogeneous broadening, $e.g.$, because of disorder or isotopic effects. Due to the different masses of isotopes, different members of the ensemble have slightly different oscillatory properties. Vibrational coherence, describing the undisturbed phase relations of two or more vibrational eigenstates can last even for solids in the pico second regime [2, 3, 21, 31–34].

Up to now the coherence effects were described from the classical point of view. Quantum mechanically, one introduces the density operator which will be described here briefly. For greater detail one is referred to the text books [25, 26]. The density operator ρ is in general defined as

$$\rho = \sum_k p_k |\Psi_k\rangle\langle\Psi_k| \tag{1.4}$$

where $|\Psi_k\rangle$ is a wave function or with Eq. 1.1 a wave packet and with the probability p_k the system will be found in the state $|\Psi_k\rangle$, where $\sum_k p_k = 1$. For of a pure state, the complete system is in

one state, otherwise it is called a mixed state.

In order to connect $\rho(x, x')$ as the density operator in the space representation to the wave packet in energy representation, a mathematical transformation, exemplified for a pure state, leads to:

$$\begin{aligned} \rho(x, x') &= \langle x|\Psi\rangle\langle\Psi|x'\rangle \\ &= \sum_{m,n} \psi_m(x)\rho_{mn}\psi_n^*(x), \end{aligned} \tag{1.5}$$

being the density matrix with elements $\rho_{mn} = c_m c_n^* e^{-\frac{i}{\hbar}(E_m - E_n)t}$. Diagonal elements

$$\rho_{nn} = \sum_k p_k \, |c_n^{(k)}|^2 \tag{1.6}$$

represent the $population$ of the energy eigenstate, since they do not include any time dependent behaviour. Only for all $|c_n^{(k)}|^2$ being zero it is possible to get a population equal to zero. All wave packet dynamic is kept in the off-diagonal elements

$$\rho_{mn} = \sum_k p_k \, c_m^{(k)} \, c_n^{(k)*} \, e^{-\frac{i}{\hbar}(E_m - E_n)t} \tag{1.7}$$

which are named $coherences$. These complex numbers are necessary to describe wave packet interferences. It is possible that the ρ_{mn} vanish, even if all $c_m^{(k)} \, c_n^{(k)*}$ are non-zero.
A matrix element $\rho_{mn} = 0$ means that interference effects smear out and the coherence between the states is lost.

Decoherence effects described earlier in the classical way can be transferred to density matrix calculations. However, the simulations described in Chs. 5 and 6 are based on a wave packet representation with complete coherence, instead of the density matrix. Thus, I refrain from the extension to decoherences, with referring to [35]. Only a brief connection shall be given: From the quantum mechanical point of view, the phase distributions in Fig. 1.2a and c) represent a minimum uncertainty wave packet. Pure dephasing in panel b) is associated in quantum mechanical calculations with the decay rate $1/T_2^*$ and dissipation in plot c) with $1/T_1$. Calculations for halogens in matrices, $e.g.$, the diatomics in molecules[1] (DIM) formalism, use in general a classical or semiclassical approach [36–38]. The latter combines a quantum wave packet with a dynamical potential obtained by classical interaction of the molecule with the environment. With reduced degrees of freedom also full quantum mechanical treatment was carried out [39–41].

Describing a real diatomic molecule, the harmonic approximation does not hold and an anharmonic potential, usually the Morse potential $V(R)$, related to the equilibrium nuclear distance R_e [27, 42] is required:

$$V(R) = D_e(1 - e^{-\alpha(R - R_e)})^2, \tag{1.8}$$

with

$$\alpha = \sqrt{\frac{\mu}{2D_e}}\omega_e, \tag{1.9}$$

where μ is the reduced mass, ω_e the harmonic eigen frequency and D_e the dissociation energy:

$$D_e = \frac{\hbar\omega_e}{4x_e}, \tag{1.10}$$

[1] The DIM formalism is based on the pair potentials between all atoms.